

Melting of Pd clusters and nanowires: A comparison study using molecular dynamics simulation

Ling Miao, Venkat R. Bhethanabotla,* and Babu Joseph

Sensors Research Laboratory, Department of Chemical Engineering, University of South Florida, Tampa, Florida 33620, USA

(Received 17 October 2004; revised manuscript received 25 August 2005; published 19 October 2005)

We present results from a molecular dynamics simulation study of a Pd cluster and a nanowire of the same diameter using the Sutton-Chen many body potential function. Changes in thermodynamic and structural properties of these two systems during heating were studied. We found that the melting temperature of the Pd nanowire of 1200 K is lower than the simulated bulk value (1760 K) but higher than that of the cluster at 1090 K. Melting behaviors were characterized by a number of thermodynamic, structural, and dynamical parameters. Surface premelting at much lower temperatures than the near first-order transition temperatures noted above was observed in both Pd systems. The surface premelting temperature range was higher for the nanowire than for the cluster. Surface melting in nanowires manifests itself as large amplitude vibrations followed by free movement of atoms in the plane perpendicular to the nanowire axis, with axial movement arising at temperatures closer to the transition temperature. Increase in nanowire diameter as well as shape change is seen to result from this axial mixing. Bond-orientational order parameters indicated that the nano-cluster retained the initial fcc structure at low temperatures. The nanowires, however, were seen to be stable at a solid structure that was close to hcp as established by bond-orientational order parameter calculations. Melting point depressions in both systems agree better with a liquid-drop model than with Pawlow's thermodynamic model.

DOI: [10.1103/PhysRevB.72.134109](https://doi.org/10.1103/PhysRevB.72.134109)

PACS number(s): 61.46.+w, 36.40.Ei, 65.80.+n, 64.70.Dv

I. INTRODUCTION

Studies of the melting process and thermodynamics properties of particles at nanometer length-scales have attracted both theoretical^{1,2} and experimental³⁻⁵ interest because of their dramatically different behavior from bulk materials.⁶ For example, it has been known that the melting temperature decreases with decreasing diameter of clusters.⁷ Transition and noble metal⁸⁻¹⁰ or alloy^{11,12} clusters and nanowires are getting more attention, mainly because of their extensive applications in catalysis and in electronic and optoelectronic nanodevices. However, many properties such as size, shape, and structure of nanomaterials affect their catalytic, optical, and electronic properties in ways that are difficult to predict.¹³ Experimentally, they have been studied using imaging¹⁴⁻¹⁶ and spectroscopic^{17,18} methods. For example, recent advances in *in situ* transmission electron microscope (TEM) techniques have allowed direct investigation of nanoparticles under realistic reaction conditions at the atomic level.¹⁹ Theoretically, the use of modeling and simulations has also substantially improved our understanding of nanomaterials in various applications. Theoretical investigations of the melting behavior of clusters and nanowires have been mostly by means of Monte Carlo (MC) and molecular dynamics (MD) computer simulations and are focused on the followings aspects: (i) investigation of the melting temperature and thermal stability during the melting process;^{20,21} (ii) the structural evolutions and mechanical properties during heating;²² and (iii) relationship of structural characteristics and size effects with temperature.^{2,23,24} For example, Wang *et al.*²¹ find that for Ti nanowires thinner than 1.2 nm, there is no clear characteristic of first-order phase transition during the melting, but a coexistence of the solid and liquid state does exist. Liu *et al.*²⁵ observed three characteristic time periods in the melting of gold isomers: disordering and reordering, surface melting, and overall melting. Lee²⁶ and co-

workers use the potential energy distribution of atoms in clusters to explain many phenomena related to the phase changes of clusters, and also find a new type of premelting mechanism in Pd₁₀ cluster.

Clusters are often considered as a bridge between individual atoms and bulk material. Recent experimental and theoretical studies demonstrated that metallic nanowires have helical multiwalled cylindrical structures²⁷ which are different from those of bulk and clusters. However, at the same time, nanowires also have some thermodynamic characteristics which are similar to either clusters or bulk because of the large surface-to-volume ratio in these nanostructures. Therefore a comparison of clusters and nanowires can provide an opportunity to better understand their behavior.

In this paper, melting characteristics of palladium nanoclusters and nanowires of comparable size are described. Pd nanoclusters and nanowires have been used widely in the design of high performance catalysts^{28,29} and nanoscale electronic devices, such as chemical sensors.³⁰⁻³² Several experiments clearly indicate that quantum behavior of metal nanoclusters is observable, and is most strongly expressed between 1 and 2 nanometers, therefore particles in that size region should be of most interest.³³ For example, Volokitin *et al.* found that 2.2 nm Pd clusters show the most significant deviations from bulk behavior at very low temperatures compared with those of 3.0, 3.6, and 15 nm diameter.³⁴ Simulation study of Pd nanomaterial provides an opportunity for further understanding its unique role in experimental phenomena. Although the size of the metallic clusters being studied in the literature ranges from tens to several thousand atoms, most efforts have been focused on sizes below 150 atoms for both Pd³⁵ and other metals. To facilitate comparison with experimental data, we investigate both melting and structural behavior of the Pd cluster with 456 atoms and comparable-sized nanowire with 1568 atoms.

TABLE I. Sutton-Chen potential parameters for Pd.

$\sigma(\text{\AA})$	$\varepsilon(10^{-3} \text{ eV})$	c	n	m
3.8907	4.1790	108.27	12	7

II. POTENTIAL MODEL AND COMPUTATIONAL METHOD

Because of the delocalized electrons in metals, the potential functions, which describe the interactions of particles, should account for the repulsive interaction between atomic cores as well as the cohesive force due to the local electron density. Several many-atom potential models were developed during the 1980s by various workers, such as the embedded atom model,³⁶ the Glue Model,³⁷ tight-binding potential with a second-momentum approximation (TB-SMA),³⁸ and Sutton-Chen (SC) potential model,³⁹ which was used in our MD simulation. The Sutton-Chen potential can be used to describe the interaction of various metals, such as Ag, Au, Ni, Cu, Pd, Pt, and Pb. It is expressed as a summation over atomic positions:

$$U = \varepsilon_{pp} \sum \left(\frac{1}{2} \sum_{j \neq i}^N \left(\frac{\sigma_{pp}}{r_{ij}} \right)^n - c \sqrt{\rho_i} \right), \quad (1)$$

where

$$\rho_i = \sum_{j \neq i}^N \left(\frac{\sigma_{pp}}{r_{ij}} \right)^m$$

is a measure of the local particle density. Here r_{ij} is the separation distance between atoms, c is a dimensionless parameter, ε_{pp} is the energy parameter, σ_{pp} is the lattice constant, and m and n are positive integers with $n > m$. The first term of the expression is a pair-wise repulsive potential, and the second term represents the metallic bonding energy between atomic cores due to the surrounding electrons. Therefore it has the same basis as the Finnis-Sinclair potential and introduces an attractive many body contribution into the total energy. This potential can reproduce bulk properties with remarkable accuracy.⁴⁰ It provides a reasonable description of small cluster properties for various transition and noble metals.^{41,42} SC potential has also been applied to model the interaction and study the properties of bimetallic alloys and metal/substrate systems.^{12,43,44} Recently, adsorbate effect of supported Pt nanoclusters was studied using the SC potential and it was found that the presence of adsorbed atoms stabilizes the surface cluster atoms under an inert gas atmosphere.⁴⁵ Values of SC parameters for Pd simulations in this paper were taken from the original work of Sutton and Chen,³⁹ as listed in Table I.

MD simulations were performed using the DL_POLY⁴⁶ package. The system was simulated under canonical (constant NVT) ensemble using the Verlet leapfrog algorithm.⁴⁷ Periodic boundary conditions were applied only in the axial direction of the nanowire. No boundary conditions were applied to the cluster. The bulk systems were studied with 3D periodic boundary conditions under constant pressure and

temperature (NPT). Both cluster and nanowire were started from face-centered-cubic (fcc) Pd bulk structure. A cutoff diameter of 2.3 nm is used to generate a spherical Pd cluster and cylindrical nanowire. This cutoff diameter is not the best way to specify the particle diameter. For the spherical cluster, the Guinier equation⁴⁸ below provides a methodology for estimating the actual radius of the cluster:

$$R_{\text{cluster}} = R_g \sqrt{5/3} + R_{\text{Pd}}, \quad (2)$$

where the first term is derived by equating the Rayleigh equation and an equation resulting from the Guinier approximation for particle scattering.^{49,50} R_g is the radius of gyration, given by

$$R_g = \sqrt{\frac{1}{N} \sum_i (R_i - R_{cm})^2}, \quad (3)$$

where $R_i - R_{cm}$ is the distance from center to the coordination point, and the sum runs over all particles. The second term in Eq. (2) is half the atomic distance in the Pd bulk, $R_{\text{Pd}} = 1.37 \text{ \AA}$. The resulting diameter calculated from Eq. (2) is about 2.6 nm, which is taken to be the diameter of the cluster in later calculations. The same 2.6 nm is taken to be the nanowire diameter.

In all the simulations reported here, a time step of 0.001 ps was used. The initial samples with atoms in ideal face-centered-cubic (fcc) positions were first relaxed by simple quenching to zero degrees. Each system was then heated with a temperature step of 50 K. The step-size was decreased to 10 K when close to the transition temperature.

III. RESULTS AND DISCUSSION

The temperature of melting transition can be identified in many ways. We first employ the variations of total potential energy and heat capacity during heating. They are shown in Fig. 1. Potential energies increase linearly with temperature in the early stage, but deviate from the linear dotted lines at higher temperatures. These deviations, associated with surface melting phenomena, will be discussed later. When close to the transition temperature, simple jumps in total potential energy, indicative of near first-order transitions, can be easily observed. Upon cooling, both the nanocluster and nanowire undergo sharp liquid-solid transitions and show rather strong hysteresis. The potential energies of the new solids are not very different from the initial ones, though structural differences are bound to prevail. We focus on the melting process in this contribution, and take the sharp jump in the energy (and the corresponding sharp peak in the heat capacity) to represent the melting temperature. Consistent with literature, we defined the melting point as the transition temperature corresponding to the temperature of observed phase change in the heating run, and the freezing point as the temperature of observed phase change in the cooling run. The presence of hysteresis in the melting/freezing transition is not unusual and is expected both theoretically^{51,52} and experimentally, as reported in the cases of Pb (Ref. 53) and Na (Ref. 1). The structural changes resulting from cooling and heating also influence the phase transition and result in hysteresis as re-

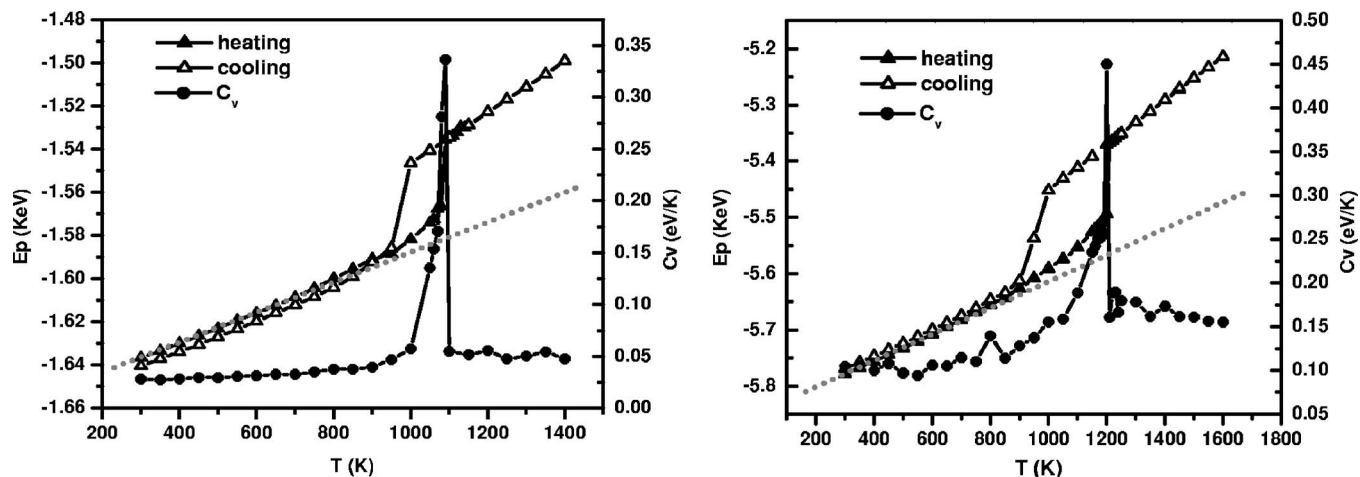


FIG. 1. Potential energy and heat capacity of the Pd (a) nanocluster (left) and (b) nanowire (right) (heating and cooling data points are on top of each other above the transition temperature, only cooling points are visible on the graphs).

ported by Chausak and Bartell in their study on freezing of Ni–Al bimetallics.⁵⁴ From the potential energy curve, we estimate the melting transition of Pd cluster to occur at 1090 K and that of the Pd nanowire at 1200 K. Both temperatures are much lower than the bulk melting temperature of 1760 K (also obtained from simulation).

The constant-volume specific heat capacity C_v is calculated by a standard formula:

$$C_v = \frac{\langle(\delta E)^2\rangle}{k_b T^2} = \frac{\langle E^2\rangle - \langle E\rangle^2}{k_b T^2}, \quad (4)$$

where E is total potential energy from the heating curve of Fig. 1, k_b is the Boltzman constant, and T is the temperature. Melting point is defined as the temperature with the maximum apparent heat capacity. The C_v curves in Figs. 1(a) and 1(b) indicate the same melting temperatures as those from E_p curves. Compared to the C_v curve before melting for the Pd cluster, that of Pd nanowire shows more structure. We also observe a small upward jump in the nanowire heating curve, after which the slope increases quickly until the large jump appears. This deviation from linearity is a result of surface melting⁵⁵ or surface reconstruction,⁵⁶ which implies that the melting process takes place in two stages, premelting and homogeneous melting. Even though this change is clearly visible from the plot for the Pd cluster, further characterization of the surface melting via dynamical variables such as the diffusion behavior and velocity autocorrelation functions revealed differences in the details of the premelting. These characterizations are discussed later in this paper. Based on the data shown in Fig. 1, we can estimate the melting temperature to be 1090 K for the Pd cluster and 1200 K for the infinitely long nanowire.

Using the above melting temperatures, the heat of fusion of Pd cluster and nanowire can be obtained by

$$\Delta H_f = H_l - H_s, \quad (5)$$

where l and s stand for the enthalpy of the liquid and solid phases. The calculated value of the heat of fusion ΔH_f for bulk, cluster, and nanowire are listed in Table II. The total

potential energy per atom is larger indicating the existence of a surface energy,⁵⁵ which can be calculated by

$$\gamma_{sv} = (E_{p_{nano}} - E_{p_{bulk}})/A, \quad (6)$$

where E_p is the potential energy of the cluster, nanowire, or bulk. A is the surface area, calculated as the surface area of a perfect sphere or cylinder, which is approximately equal to the surface area of cluster and nanowire at 300 K. For the Pd cluster system, the difference of potential energy at 300 K is 29.873 kJ/mol. Hence we obtain a surface energy of 1.328 J/m². Similarly for nanowire, we have $\gamma_{sv} = 1.393$ J/m². Therefore we see that the Pd nanowire has larger energy per unit surface and higher heat of fusion than the comparable Pd cluster, which in turn implies the higher melting temperature.

Shape changes of the Pd nanocluster and nanowire were monitored by calculating the radius of gyration using Eq. (3). Considering that the infinitely long nanowire is symmetrical about the z axis, and we are only interested in the shape variance in the x - y plane, we use two-dimensional R_g for the Pd nanowire, which is to say only the distance from each atom to the z axis is utilized.

Fig. 2 shows the temperature dependence of the radius of gyration R_g of the Pd nanocluster and nanowire. In both cases, R_g has an upward jump at the melting transition, indicating that cluster and nanowire behave similarly in expanding to a wider shape.

TABLE II. Thermodynamic properties for Pd bulk, cluster, and nanowire.

	T_m (K)	ΔH_f (kJ/mol)	γ_{sv} (J/m ²) ($T=300$ K)
Bulk (simulation)	1760	16.83	
Bulk (experiment)	1825 (Ref. 73)	16.7 (Ref. 74)	1.808 (Ref. 73)
Pd cluster	1090	6.71	1.328
Pd nanowire	1200	7.36	1.393

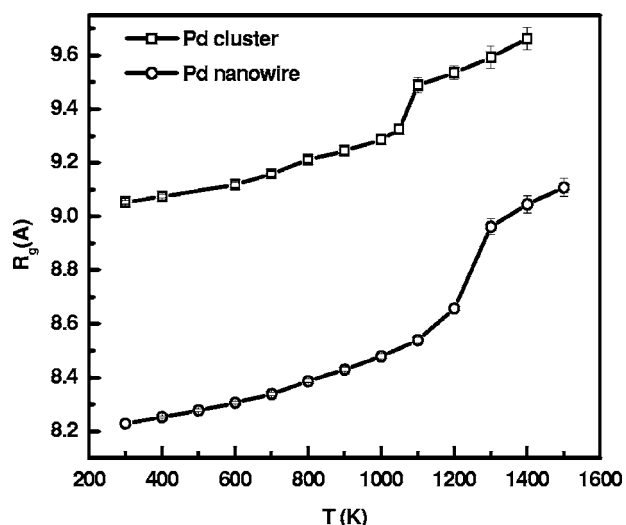


FIG. 2. Radius of gyration vs temperature for Pd cluster and Pd nanowire with repeating unit of length=5.6 nm.

The structural features of the nanowire upon heating were further explored by visualization through snap shots and trajectory plots to understand the differences in the surface premelting phenomenon between the nanowire and cluster. Fig. 3(a) shows sample projected coordinates, on to the plane parallel to the nanowire axis, of each atom at two temperatures of 700 and 800 K, as blue and red dots, as well as a dashed line connecting each of the atomic positions at the two temperatures. What is apparent is an oscillatory motion in the plane perpendicular to the nanowire axis, with atoms mostly retaining their positions through the simulation duration. Very few surface atoms exhibit large movement along the wire axis, crossing different planes. This surface atomic movement was found to be rarer at temperatures lower than the 700–800 K shown in this figure. While a bit more difficult to see from Fig. 3(b), similar behavior is exhibited at the slightly higher temperatures of 900 and 1000 K. The top view in Fig. 3(b) shows more movement at the surface than towards the center of the wire. Analysis of these and similar plots along with trajectory visualizations have provided a picture of the surface premelting of one where the nanowire exhibits increasingly freer motion of the surface atoms in the plane perpendicular to the nanowire axis at temperatures much below the near first-order transition temperature, with the degree of freedom parallel to the nanowire axis available at higher temperatures, closer to the transition temperature. The surface premelting is further characterized by a shrinking solidlike core of the nanowire, as the temperature increases to the transition point. This physical picture is consistent with the deviation of the potential energy curve from linearity as shown in Fig. 1(b), however, these details of the structural and dynamical changes are not apparent from that plot. Indeed, the potential energy curve for the near-spherical nanocluster shown in Fig. 1(a) exhibits similar behavior, however, details of the surface premelting are quite different, a difference arising from the difference in the geometry. It should be noted here that both nanoclusters and nanowires of various metals have been synthesized by a variety of templating and other solution techniques, and it is possible to

experimentally observe these differences in melting behavior upon heating of these nanomaterials. No such experiments have been reported in the literature to our knowledge.

Components of the velocity autocorrelation function in cylindrical coordinates were calculated as functions of distance from the nanowire axis to characterize atomic motion in the surface premelting regime. v_θ and v_z characterize movement in the x - y plane and in the z direction. Fig. 4 shows the correlation of v_θ and v_z with time at 800 K. The five curves in both plots represent correlated atoms at different distances from the center with 1 being the closest and 5 the farthest. The wire was partitioned into these five shells with $dR=2.77$ Å based on the initial equilibrium atomic positions (time origins of the time-correlation function calculations), with dR chosen to be close to the interatomic distance in bulk solid Pd of about 2.75 Å. Atoms stayed within their shells for the duration of the correlation time, and beyond, justifying these calculations to further understand the surface melting phenomenon.

Both components of the correlation functions for the inner shells exhibit rebounding oscillations that decay with time, indicative of localization at lattice sites. Comparing the two plots, v_θ has shorter correlation time and much larger depth of the minima than v_z , which implies larger amplitude tangential vibrations than axial. Behavior of atoms in the outer shells (especially, the outermost shell) is significantly different, at this temperature of 800 K, with surface premelting apparent. Nearly liquidlike motion is inferred from the single damped oscillation with one minimum before de-correlation with time occurs. While results at the one temperature of 800 K are shown in Fig. 4 to illustrate the surface premelting phenomenon, v_θ and v_z calculated at the other temperature corroborate the arguments developed here. At temperatures higher than 900 K, axial movement is larger while the tangential oscillations are dampened. The wire diameter increases with temperature as a result of these movements.

Surface melting is observed frequently in simulations of nanoparticles. Surface atoms melt at temperatures below the transition temperature, and then the quasiliquid skin continuously grows thicker as the temperature increases. The inner regions stay ordered until the transition temperature. The temperature at which the film thickness diverges to the entire system size is thought of as the cluster melting point. However, for ultrathin gold nanowires, Wang *et al.*²⁷ found the interior melting temperature to be lower than that of the surface, indicating that the melting actually starts from inside, exhibiting no surface melting behavior.

Snapshots of atomic positions projected onto a plane (perpendicular to the axis in the nanowire case) are shown in Fig. 5. These provide evidence for surface melting in both the Pd cluster and nanowire cases.

Further evidence of surface melting in both cluster and wire is obtained from self-diffusion coefficients calculated as functions of radial distance using mean-square displacements. As in the calculation of the velocity autocorrelation functions, the atoms were assigned to bins based on their initial positions at the end of the equilibration period. The mean-square displacements for each shell were then generated by averaging over a 25 ps trajectory with sampling done every 0.1 ps. Averages taken over a 25 ps trajectory with

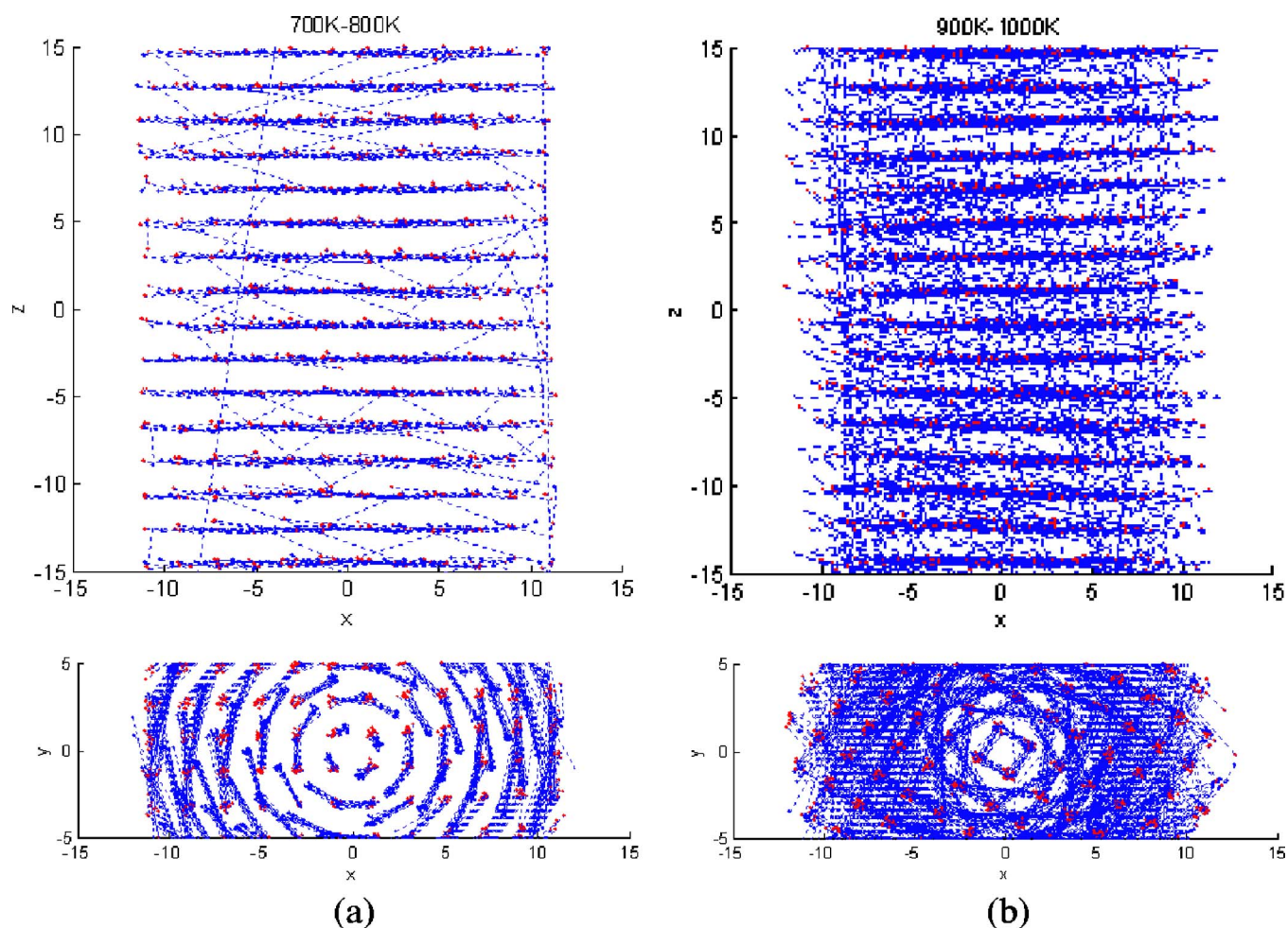


FIG. 3. (Color online) Snapshots of equilibrated atomic positions, shown as projected coordinates in planes parallel (upper) and perpendicular (lower) to (a) the nanowire axis. Blue dots are for 700 K and red dots are for 800 K, with the blue dashed lines connecting the same atoms at the two temperatures. Similar plot for (b) 900 and 1000 K.

different origins gave the same result which is indicative of a system that is truly in equilibrium. The self-diffusion coefficients were calculated for each radial shell at various temperatures using the equation

$$D = \frac{1}{6N} \lim_{t \rightarrow \infty} \frac{d}{dt} \sum_i [r_i(t) - r_i(0)]^2 \quad (7)$$

These are shown in Fig. 6. In all the cases, we find the diffusivities of outer shells to be higher than those of the inner ones. If $D_1 \sim D_5$ denote self-diffusion coefficients of these shells from inner to outer, we found that at lower temperatures, both clusters and nanowires have similar self-diffusion coefficients of the order of $10^{-3} \text{ \AA}^2/\text{ps}$. Atoms in the outer shells have larger diffusion coefficient than the atoms closer to the core atoms. As the temperature increases further, the diffusion coefficient of the outermost shell, D_5 , first starts to increase rapidly. This is followed by an increase of D_4 , while D_1, D_2, D_3 retain their values from the lower temperatures. This state is maintained until the melting transition temperatures are approached. The larger diffusion coefficients in outer shells and relatively static state of inner shells at temperatures below the transition temperatures sup-

port the existence of surface melting in both Pd cluster and nanowire. Atoms on the surface have weaker restraining forces than the core atoms. Although surface melting in some sense is not necessarily a diffusive process, it can be considered a complex phenomenon involving cooperative motion.⁵⁶ According to the Lindemann criterion, the phase transition occurs when atomic motion exceeds 10–15% of interatomic distance. From the variation of the diffusion coefficients in various bins, we can infer a continuous layer-by-layer melting as the atomic displacements meet the Lindemann criterion in a layer-by-layer manner, until the criterion is met for the remaining solid core all at once, at the near first order transition temperature. From the diffusion plots, together with the variations of potential energies and heat capacity curves in Fig. 1, we estimate the surface melting regions of the Pd cluster and nanowire to start at about 700–800 K, and 800–900 K, respectively. At melting points, diffusion coefficients of all the shells exhibit large jumps of similar magnitude, indicating the phase transitions from solid to liquid.

Structural properties and changes in them during heating are of interest in understanding mechanical and catalytic properties of materials. Experimental observations include changes in the lattice parameter, surface coordination, and

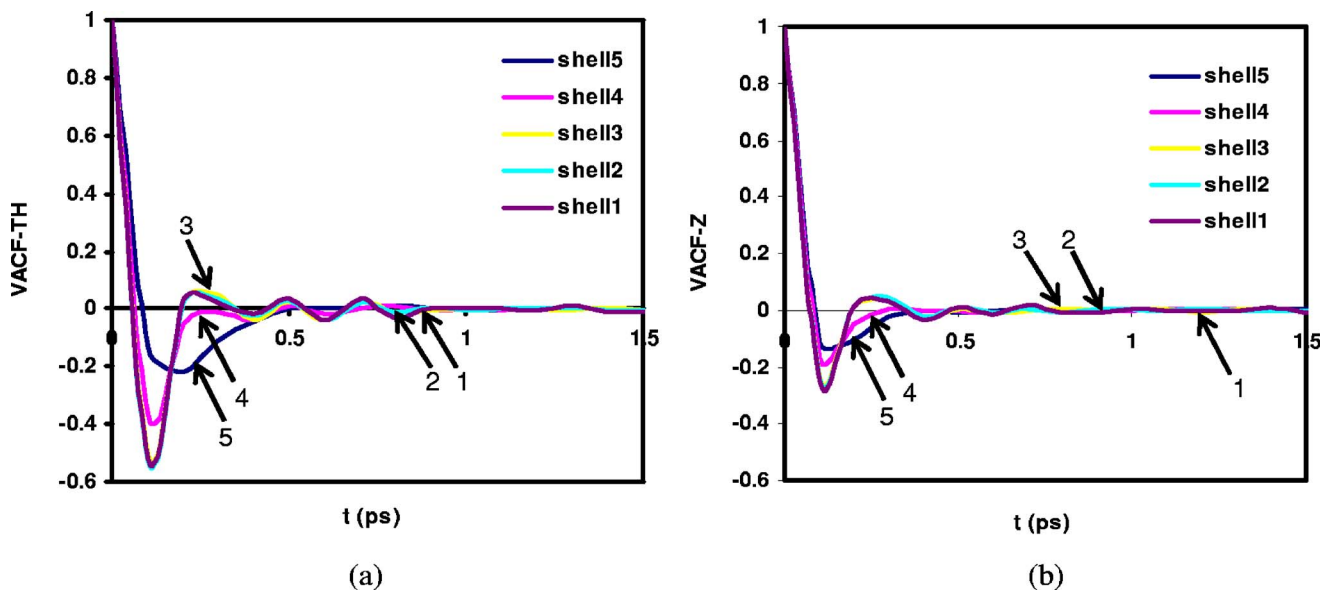


FIG. 4. (Color online) Velocity autocorrelation functions for atoms in different shells of the Pd nanowire at 800 K. Shell 1 is the closest to the wire axis and shell 5 is the farthest. (a) v_{θ} and (b) v_z .

structural fluctuations. Some theoretical calculations include detailed studies of the topology and structural stability. Many small clusters, with special numbers of atoms, so-called magic numbers, have proven to be more stable than others.⁵⁷ The change in crystallographic structure can be attributed to surface energy. Icosahedral Pd clusters with 13, 55, and 147 atoms are examples. The geometry of these extremely small clusters with unique minimum energy has been extensively studied.^{22,35} In this work, we pay attention to the time evolution of the structures during heating by investigating two parameters: atomic number distribution along the z direction (a Cartesian direction, along the wire axis for the nanowire) and bond-orientational order parameters.

The atomic number distribution $N(z)$ for each element is defined as

$$N(z) = \left\langle \sum_i \delta(z_i - z) \right\rangle, \quad (8)$$

$N(z)$ is a good way to look at the structural features during heating of the spherical cluster and one-dimensional nanowire of similar diameter. Plots in Fig. 7 show the distribution of Pd atoms along the z axis at different temperatures. In the solid phase, atoms have higher distribution only at certain distances from the center, forming many sharp peaks. Those peaks become wider and shorter upon heating and finally disappear due to the uniformly distributed atoms in liquid phase. This expected behavior in $N(z)$ is seen in the Pd cluster case, as shown in Fig. 7. In contrast, Fig. 8 for the nanowire exhibits complicated structural features. Longer wavelength variations in the $N(z)$ distribution are introduced due to increased amplitudes of oscillations of the atoms in ordered zones. The ordered zones appear to move along the wire as we approach the transition, with the possibility of such movement with time, at a single temperature. While the lowest temperature shown in Fig. 8 is 600 K, we have seen

this behavior at the lowest temperature simulated, of 100 K. This extremely interesting behavior could be an artifact of the periodic boundary conditions. To explore this further, we have repeated the simulations with a wire that is twice in length. Results indicated that the longer wavelength ordering of zones is possible in the surface-melting regime, and is enhanced as the transition temperature is approached. However, the periodic structures observed in the low temperature solid structures such as shown in Fig. 8(a) have disappeared. None of the melting properties we report in this paper were affected by the doubling of the wire length. We conclude that there exists the possibility of ordered zones in Pd nanowires at close-to-transition temperatures, and that this phenomenon should be explored with simulations of much longer wires, to eliminate all effects of periodic boundary conditions. To explore the possibility of lower density in the valley (and consequent higher density in the peaks) we have utilized the two-dimensional radius of gyration, as defined previously for the nanowire. Calculations of these radii in the peaks and

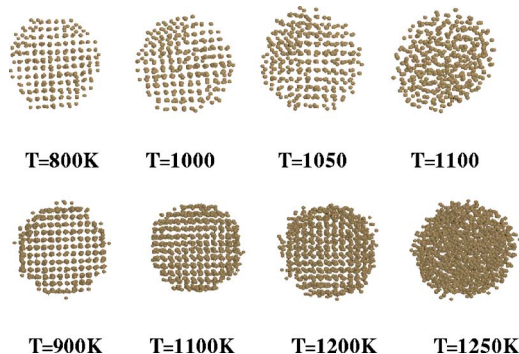


FIG. 5. (Color online) (a). Snapshots of the projected atomic positions of the 456 Pd atom clusters at different T . (b). Same as (a) but for the 1568 atom Pd nanowire projected onto a plane perpendicular to the axis.

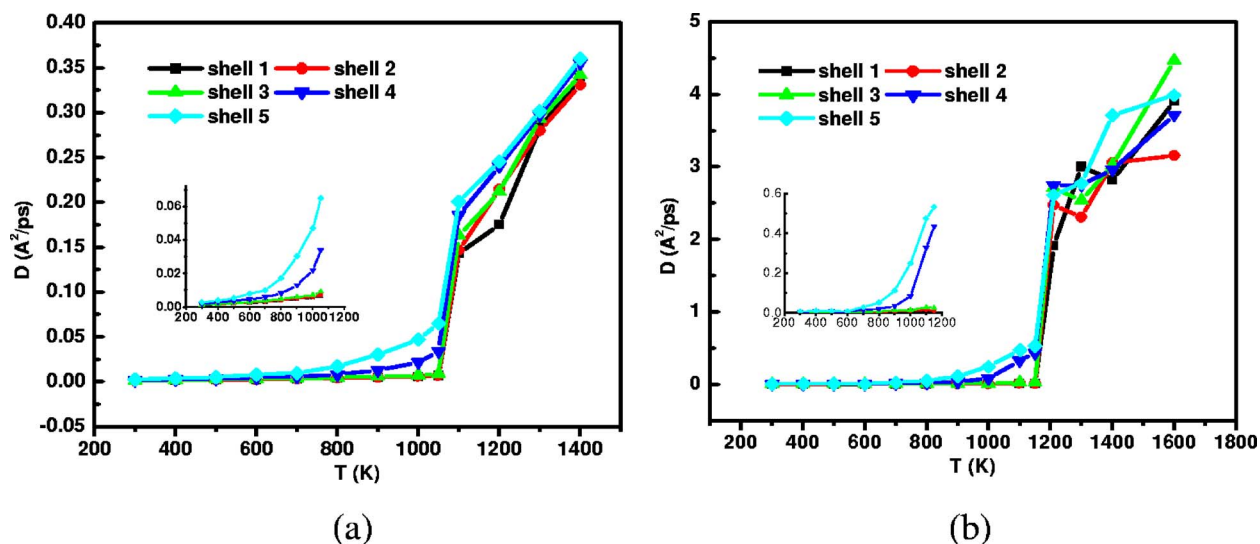


FIG. 6. (Color online) Self-diffusion coefficient for atoms in different radial shells at various temperatures: (a) Pd cluster and (b) Pd nanowire.

valleys yielded nearly the same numerical values in the solid phase, indicating that these features are caused by larger amplitude oscillations of the atoms.

The bond-orientational order parameters (BOP) method⁵⁸ was applied to quantify structural evolution of the clusters and nanowires crystallographically, as well as to distinguish between liquidlike and solidlike states. Bonds are defined as the vectors joining a pair of neighboring atoms with an interatomic distance less than a specified cutoff radius. The cutoff distance is usually chosen as the position of the first minimum in the pair correlation function, which is about 3.36 Å in this case. Associated with every bond is a set of numbers called local bond-orientational order parameters:

$$Q_{lm}(r) = Y_{lm}[\theta(r), \phi(r)], \quad (9)$$

where $Y_{lm}(\theta, \phi)$ are spherical harmonics and $\theta(r)$ and $\phi(r)$ are the polar angle and azimuthal angles of vector r with respect to an arbitrary reference frame. Only even- l spherical harmonics are considered, which are invariant under inversion. A global bond-orientational order parameter $\bar{Q}_{lm}(r)$ can be defined by averaging $\bar{Q}_{lm}(r)$ over all bonds in the system:

$$\bar{Q}_{lm} = \frac{1}{N_b} \sum Q_{lm}(r), \quad (10)$$

where N_b is the number of bonds. To let $\bar{Q}_{lm}(r)$ not depend on the choice of reference frame, a second-order invariant is constructed as

$$Q_l = \left(\frac{4\pi}{2l+1} \sum |\bar{Q}_{lm}|^2 \right)^{1/2}, \quad (11)$$

and a third-order invariant is constructed as

$$W_l = \sum_{m_1, m_2, m_3} \begin{pmatrix} l & l & l \\ m_1 & m_2 & m_3 \end{pmatrix} \bar{Q}_{lm_1} \bar{Q}_{lm_2} \bar{Q}_{lm_3}. \quad (12)$$

The term in the bracket is a Wigner-3j symbol.⁵⁹ Furthermore, a reduced order parameter \hat{W}_l is defined so that it is not sensitive to the precise definition of the nearest neighbor of a particle:

$$\hat{W}_l = W_l / \left(\sum |\bar{Q}_{lm}|^2 \right)^{3/2}. \quad (13)$$

The values of these bond-orientational order parameters for some common crystal structures are listed in Table III.

Because of symmetry, the first nonzero values occur for $l=4$ in the cluster with cubic symmetry and for $l=6$ in clusters with icosahedral symmetry. We used the four bond-orientational order parameters $Q_4, Q_6, \hat{W}_4, \hat{W}_6$ together to

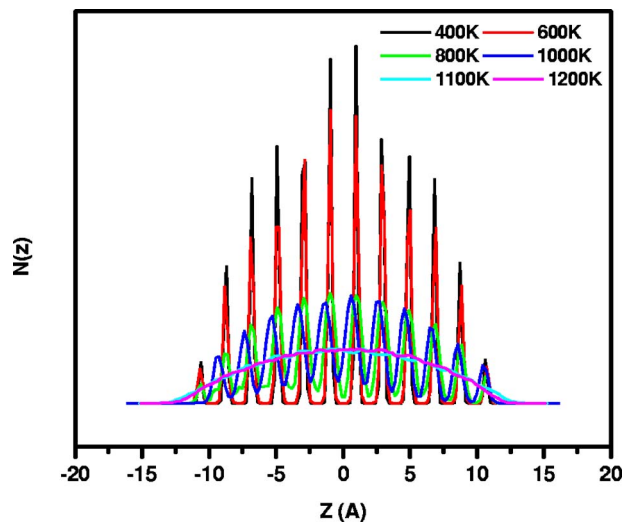


FIG. 7. (Color online) Comparison of Pd atomic distributions of Pd cluster along a Cartesian coordinate (z) at different temperatures.

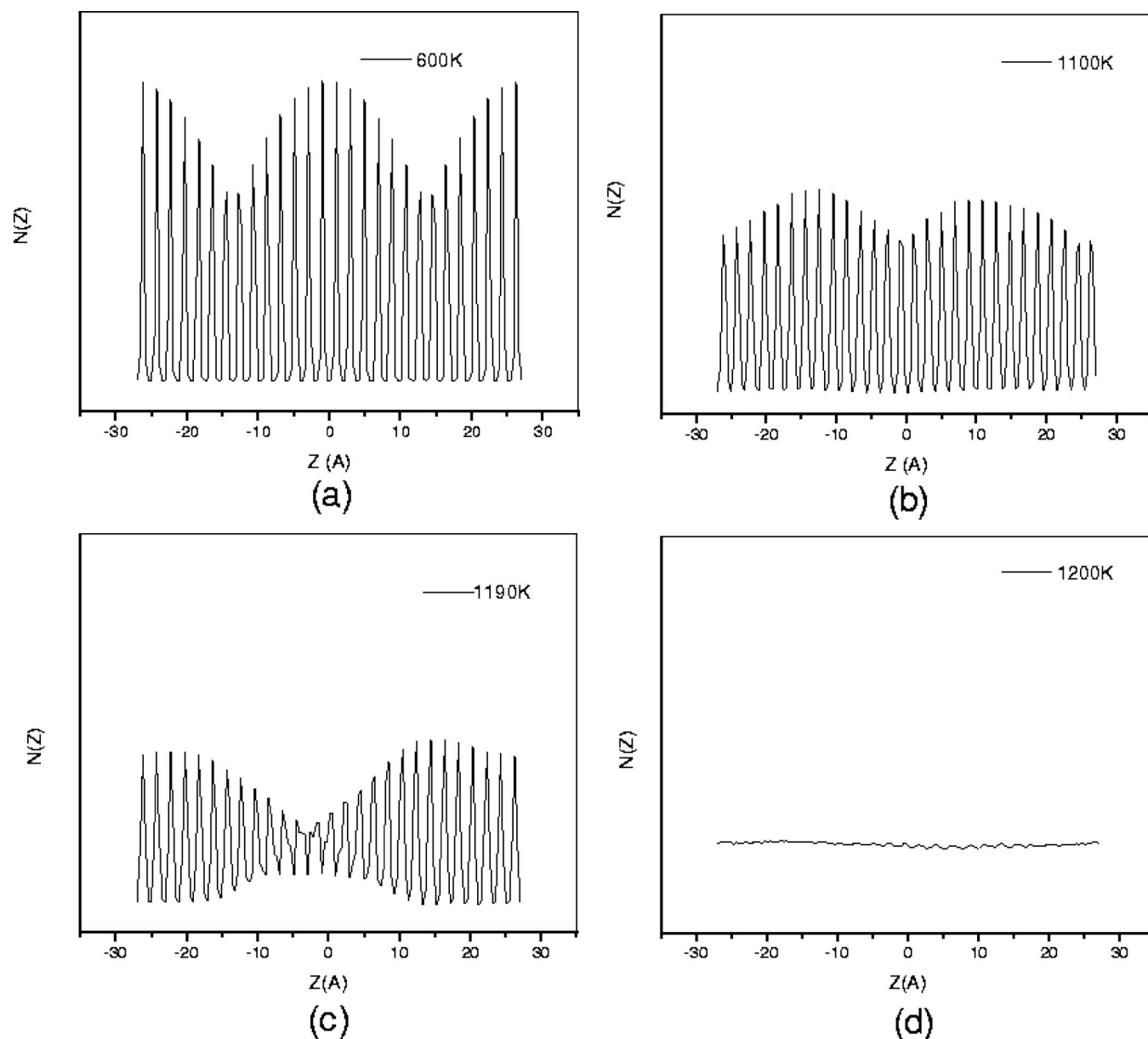


FIG. 8. (a–d). Comparison of Pd atomic distribution along a Cartesian coordinate (z) in the Pd nanowire at different temperatures.

identify structures. Note that Q is of the same order of magnitude for all crystal structures of interest, which makes it less useful for distinguishing different crystal structures compared to \hat{W} . But Q_6 is useful to identify phase transitions,

TABLE III. Bond-orientational order parameters for a number of simple cluster geometries (Ref. 58).

Geometry	Q_4	Q_6	\hat{W}_4	\hat{W}_6
Icosahedra	0	0.66332	0	0.16975
fcc	0.19094	0.57452	0.15932	0.01316
hcp	0.09722	0.48476	0.13410	0.01244
bcc	0.03637	0.51069	0.15932	0.01316
Liquid	0	0	0	0

since it has a larger value than other parameters and decreases quickly to zero when the system becomes liquid. Considering the surface effect in nanomaterials and to get more accurate answers to monitor global structural changes, we calculated bond-orientational order parameters for internal atoms, surface atoms, and all atoms in the systems.

The time averaged bond-orientational order parameters of the internal atoms, surface atoms, and the entire Pd nanowire system are plotted in Fig. 9(a). We see that only the second-order invariants (Q values) differ when the surface atoms are excluded, while the third-order invariants (\hat{W} values) are not affected. This is because Q is more sensitive to the number of the nearest neighbors. Fig. 9(b) shows the bond-orientational order parameter comparison between the Pd cluster and the Pd nanowire. All the parameters drop abruptly to zero at the transition temperature. These changes

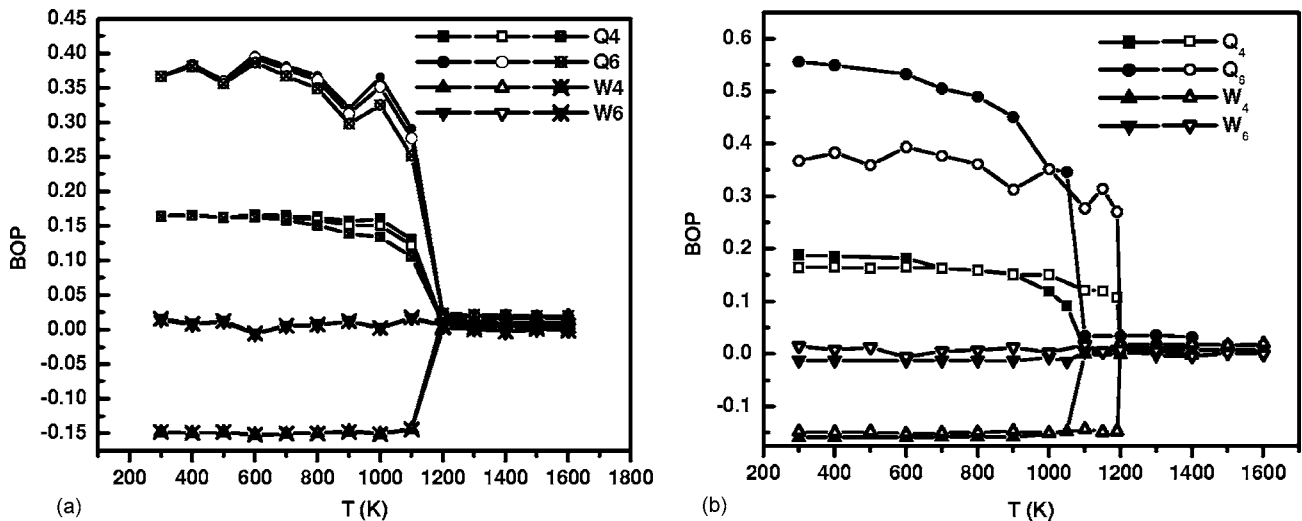


FIG. 9. (a). Temperature dependence of average bond-orientational order parameters for atoms in Pd nanowire. Filled, unfilled, and unfilled with a cross symbols correspond to the average bond-orientational order parameters for internal atoms, all atoms, and surface atoms, respectively. (b). Temperature dependence of average bond-orientational order parameters for the Pd cluster with 456 atoms and Pd nanowire with 1568 atoms during heating. Filled and unfilled symbols represent cluster and nanowire, respectively.

are more obvious in Q_6 . Even though the Pd cluster retains the fcc structure at lower temperatures, the time averaged global bond-orientational order parameters show that the Pd nanowire moves away from the starting fcc structure, which is consistent with what we have seen in the $N(z)$ plots. The correlation plot for \hat{W}_6 as a function of Q_6 is shown in Fig. 10, where the red dots are the values for perfect crystals. We use Q_6 because it changes significantly with temperature. We see from the time averaged bond-orientational order parameters that at low temperature, the Pd nanowire no longer has fcc structure, instead it forms some structure beyond regular crystal geometries. From Fig. 10, we observe that the nanowire undergoes a rapid structural change during the annealing process, after that it maintains a nonregular structure at low temperatures before the phase transition. Unlike the nanowire, the cluster goes through possible structural changes in the same temperature range, reflected by the decreasing rate of change of Q_6 . Calculated values of Q_6 are sensitive to the number and positions of the surface atoms. More rapid changes in the number and positions of these surface atoms in the cluster compared to the cylindrical wire with periodic boundary conditions could explain this behavior of Q_6 . \hat{W}_6 has more fluctuations in the nanowire than the cluster, indicating frequent symmetry changes.⁵⁸

In our simulations, we have chosen the bulk, fcc structure for the starting configurations of the low temperature solid nanocluster and nanowire. It is difficult to establish the true low temperature solid structures of these nanomaterials from molecular dynamics simulations. One cannot be certain that the bulk fcc structure is a reasonable starting structure, although other studies have utilized bulk structures for starting configurations of nanomaterials.^{48,55,60} Some insights can be gained by starting the simulations from other hypothetical structures, such as the hcp, and a glassy structure that results from the first heating/cooling cycle of the fcc-started simulation. To establish the reasonableness of our fcc-started

simulations, we have repeated the heating/cooling simulations with an hcp initial structure and the glassy structure obtained at 300 K upon completion of the first fcc-started MD run after a full heating/cooling cycle. Some experimental⁶¹ and simulation²⁰ evidence for the possibility of hcp structures in nanoclusters exists in the literature, with less known about nanowires. With minor variations accounted for by the differences in numbers of atoms (mandated by the differences in starting configurations for different close packed structures of the same diameter), we have found that the melting points are essentially the same as those obtained from the fcc-started simulation. While the hcp-started cluster appeared to be stable at low temperatures, it undergoes a less sharp transition (while yielding nearly the

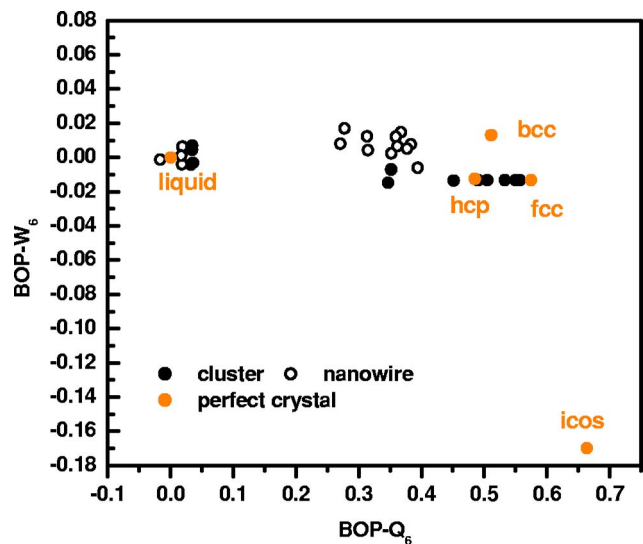


FIG. 10. (Color online) Correlation plot for bond-orientational order parameters W_6 as a function of Q_6 . Symbols are at 100 K intervals starting at 300 K.

same melting point), perhaps due to structural rearrangement in the solids near melting temperature and/or enhanced surface melting as compared to the fcc-started cluster. The hcp-started nanowire, on the other hand, rapidly rearranged to a less-ordered structure at low temperatures as in the fcc case and showed a sharper melting transition, with an identical melting point as the fcc-started wire. The annealed solid structures during cooling, of both cluster and wire, did not track potential energies of the heating run, indicating that the fcc starting configuration is perhaps closer to the true structure of both the cluster and the wire. Nearly identical melting points and potential energy curves were found from the second heating/cooling cycle of the fcc-started cluster and wire, indicating that the cycle, including hysteresis, is repeatable. This gives further support to the choice of the fcc structure in our low temperature solid starting configurations. Coupled with the results for the bond orientational order parameters presented in Fig. 10, we conclude that the chosen fcc starting configurations are reasonable in this study. Generally, prior to melting, both systems have trends towards disorder as the number of unclassified bond orientations increases. The classifications of local atoms during heating can be improved by studying CNA (common neighbor analysis) signatures, as shown in the work from Hendy *et al.*⁶²

IV. MELTING MODEL COMPARISON

Melting behavior, especially melting temperature, of clusters and nanowires will depend on their size. The study of size effects on melting of metallic nanoparticles has been explored both experimentally and theoretically,^{4,63–65} and a large number of data have been established. Models for the size-dependent melting point depression for different materials have been established based on various assumptions, such as many outstanding classic thermodynamics models^{6,66–69} and other models, like surface-phonon instability model,⁷⁰ bond order-length-strength (OLS) model,⁷¹ and liquid-drop-like model.⁷² The general result of these theories is that melting temperature of small particles decreases linearly or quasilinearly with the decreasing of their diameters. In this section, we compare our simulated results with two of the models.

The thermodynamics model was first proposed by Pawlow⁶⁶ in 1909, it is based on equating the Gibbs free energies of solid and liquid spherical clusters, assuming constant pressure conditions, with the resulting equation:

$$\frac{T^b - T_c(R)}{T^b} = \frac{2}{\rho_s L^b R} \left[\gamma_{sv} - \left(\frac{\rho_s}{\rho_l} \right)^{2/3} \gamma_{lv} \right], \quad (14)$$

where T^b and L^b are the bulk melting temperature and bulk latent heat of melting, ρ is the mass density, γ_{sv} and γ_{lv} are the solid-vapor and liquid-vapor bulk material interfacial energies, respectively. The simulated melting point depression [$T_b - T_c(2.6 \text{ nm})$] of 670 K is higher than the 278 K predicted by the above model. It has been pointed out in the literature that the $1/R$ behavior is approximately correct for clusters of sufficiently large size.^{7,53}

For a nanowire, a similar procedure can be applied by equating the Gibbs free energies per unit length of solid and

liquid at constant temperature and pressure. Gülseren²⁴ developed a model for the melting temperature $T_{nw}(R)$ of nanowires:

$$\frac{T^b - T_{nw}(R)}{T^b} = \frac{1}{\rho_s L^b R} \left[\gamma_{sv} - \left(\frac{\rho_s}{\rho_l} \right)^{1/2} \gamma_{lv} \right]. \quad (15)$$

These two models have been shown to agree with simulation results in Gülseren's Pb clusters and wires constructed from (110) planes with more than 1100 atoms in the systems.

From Eqs. (14) and (15), we see that since ρ_s/ρ_l is close to 1, the depression of melting temperature of a spherical cluster should be approximately twice that of the corresponding amount for a nanowire. Using $\gamma_{sv}=1.808 \text{ J/m}^2$, $\gamma_{lv}=1.480 \text{ J/m}^2$, $\rho_s=0.0681 \text{ atom/A}^3$, $\rho_l=0.0594 \text{ atom/A}^3$, and $L^b=16.69 \text{ kJ/mole}$, the calculated depressions of melting temperatures are 160 and 278 K for the Pd nanowire and cluster, respectively, giving a ratio of 1.7. However, our simulation results yield a ratio of 1.2. This discrepancy may be due to the many assumptions in the model and the simulation, for example, the surface energy anisotropy of the solid is not taken into account, and the possibility of inhomogeneous phases is also neglected in the model. The same discrepancies between model and simulation results exist in other previous work.^{48,55} The accuracy of these models appears to be better for larger clusters and nanowires than simulated here. It should also be noted that significant variation exists in the literature for values of the interfacial energies. Also, using the simulated interfacial energies for the clusters and wires, and not the bulk values, would improve comparison with Pawlow's model.

The other scaling law⁷² for size-dependent melting is based on the liquid-drop model and empirical relations between surface energy, cohesive energy, and size-dependent melting temperature. According to this model, the cohesive energy of N -atom nanoparticles can be represented by volume and surface dependent terms. For a spherical nanoparticle of diameter d , the expression for the cohesive energy per atom can be written as

$$a_{v,d} = a_v - \frac{6v_0\gamma}{d}, \quad (16)$$

where $a_{v,d}$ and a_v are the cohesive energy per atom in the cluster and in the bulk, v_0 is the atomic volume, and γ is surface energy of solid-vapor interface. Using empirical relations between cohesive energy and melting temperature for both bulk and nanoparticles, the melting temperature of nanoparticles can be calculated by

$$\frac{T_c(R)}{T^b} = 1 - \frac{6v_0}{0.0005736d} \left(\frac{\gamma}{T^b} \right) = 1 - \frac{\beta}{d}, \quad (17)$$

where

$$\beta = \frac{6v_0}{0.0005736} \left(\frac{\gamma}{T^b} \right).$$

The value of β can be calculated from the known values of v_0 , γ , and T^b . Using $\beta=0.9517 \text{ nm}$ for Pd in Eq. (17), we get the melting point depression of the Pd cluster of 669 K, which compares well with our simulated value of 670 K.

This favorable comparison is consistent with other work mentioned previously.^{48,55} Using the same model for the melting of thin wires, the size-dependent melting temperature of a nanowire can be described by⁷³

$$\frac{T_{nw}(R)}{T^b} = 1 - \frac{2\beta}{3d}. \quad (18)$$

From this, the depression of melting temperature of the nanowire is 446 K, smaller than our simulated result of 560 K. This relation described in Eq. (18) has some similarity to the model of Gülseren, described previously, except that the depression of melting temperature of a nanowire is 2/3 of the depression of the spherical nanocluster. That is

$$\frac{T^b - T_c(R)}{T^b - T_{nw}(R)} = 1.5. \quad (19)$$

This number is closer to our simulation result of 1.2 than that from Pawlow's model.

V. CONCLUSIONS

The simulation studies of this work indicate that the Pd nanowire has lower melting temperature than Pd bulk but higher than the same diameter Pd cluster. Both Pd nanowires and nanoclusters exhibit surface premelting, the structural and dynamical nature of which is somewhat different. These differences are fully characterized by several thermody-

namic, structural, and dynamic variables in this study. The general picture that emerges is that the surface premelting behavior for the cluster is similar to that of other noble and transition metal nanoclusters. The nanowire exhibits a higher premelting temperature range, and dynamical behavior characterized by increased movement of atoms in the plane perpendicular to the axis followed by increased movement across these planes, as the temperature approaches the transition temperature. A quasiliquid skin grows from the surface in the radial direction for both cluster and wire, in the surface premelting regime, followed by the breakdown of order in the remaining solid core at the transition temperature. Bond-orientational order parameters indicated that the cluster retains the initial fcc structure, whereas the nanowire appears stable in a structure close to the hcp, in the solid phase, before melting. Melting points of studied cluster and wire were characterized particularly well by the liquid-drop model for size-dependent melting.

ACKNOWLEDGMENTS

Partial support was provided by NASA-Glenn via FSEC, Florida. The Daresbury Laboratory provided the DL_POLY package and the Research Computing Core Facility at the University of South Florida provided computational resources, both of which are gratefully acknowledged. The authors thank Subramanian K.R.S.S. for some valuable discussions.

*Corresponding author. Electronic address: venkat@eng.usf.edu

¹M. Schmidt, R. Kusche, W. Kronmüller, B. Von Issendorff, and H. Haberland, *Phys. Rev. Lett.* **79**, 99 (1997).

²F. Ercolessi, W. Andreoni, and E. Tosatti, *Phys. Rev. Lett.* **66**, 911 (1991).

³M. Schmidt, R. Kusche, B. V. Issendorff, and H. Haberland, *Nature (London)* **393**, 238 (1998).

⁴S. L. Lai, J. Y. Guo, V. Petrova, G. Ramanath, and L. H. Allen, *Phys. Rev. Lett.* **77**, 99 (1996).

⁵K. F. Peters, J. B. Cohen and Y-W Chung, *Phys. Rev. B* **57**, 13430 (1998).

⁶R. R. Couchman, *Philos. Mag. A* **40**, 637 (1979).

⁷J. P. Borel, *Surf. Sci.* **106**, 1 (1981).

⁸R. C. Longo, *Surf. Sci.* **459**, L441 (2000).

⁹T. X. Li, Y. L. Ji, S. W. Yu, and G. H. Wang, *Solid State Commun.* **116**, 547 (2000).

¹⁰C. Rey, L. J. Gallego, J. Garcia-Rodeja, J. A. Alonso, and M. P. Iniguez, *Phys. Rev. B* **48**, 8253 (1993).

¹¹Y. Shimizu, K. S. Ikeda, and S. I. Sawada, *Phys. Rev. B* **64**, 075412 (2001).

¹²S. P. Huang and P. B. Balbuena, *J. Phys. Chem. B* **106**, 7225 (2002).

¹³P. L. Hansen, J. B. Wagner, S. Helveg, J. R. Rostrup-Nielsen, B. S. Clausen, and H. Topsøe, *Science* **295**, 2053 (2002).

¹⁴T. W. Hansen, J. B. Wagner, P. L. Hansen, S. Dahl, H. Topsøe, and C. J. H. Jacobson, *Science* **294**, 1508 (2001).

¹⁵Y. Kondo and K. Takayanagi, *Science* **289**, 606 (2000).

¹⁶A. Mikkelsen, N. Skold, L. Ouattara, M. Borgstrom, J. N. Andersen, L. Samuelson, W. Seifert, and E. Lundgren, *Nat. Mater.* **3**, 519 (2004).

¹⁷J. Wang, H. F. M. Boelens, M. B. Thathagar, and G. Rothenberg, *ChemPhysChem* **5**, 93 (2004).

¹⁸B. L. M. Hendriksen and J. W. M. Frenken, *Phys. Rev. Lett.* **89**, 046101 (2002).

¹⁹S. Helveg, C. Lopez-Cartes, J. Sehested, P. L. Hansen, B. S. Clausen, J. R. Rostrup-Nielsen, F. Abild-Pedersen, and J. K. Nørskov, *Nature (London)* **427**, 426 (2004).

²⁰Y. G. Chushak and L. S. Bartell, *J. Phys. Chem. B* **105**, 11605 (2001).

²¹B. Wang, G. Wang, X. Chen, and J. Zhao, *Phys. Rev. B* **67**, 193403 (2003).

²²C. L. Cleveland, W. D. Luedtke, and U. Landman, *Phys. Rev. B* **60**, 5065 (1999).

²³S. Valkealahti and M. Manninen, *Phys. Rev. B* **45**, 9459 (1992).

²⁴O. Gülseren, F. Ercolessi, and E. Tosatti, *Phys. Rev. B* **51**, 7377 (1995).

²⁵H. B. Liu, J. A. Ascencio, M. P. Alvarez, and M. J. Yacaman, *Surf. Sci.* **491**, 88 (2001).

²⁶Y. J. Lee, E. K. Lee, S. Kim, and R. M. Nieminen, *Phys. Rev. Lett.* **86**, 999 (2001).

²⁷J. Wang, X. Chen, G. Wang, B. Wang, W. Lu, and J. Zhao, *Phys. Rev. B* **66**, 085408 (2002).

²⁸G. Schmid, S. Emde, V. Maihack, W. MeyerZaika, and S. Pechel, *J. Mol. Catal. A: Chem.* **107**, 95 (1996).

- ²⁹H.-U. Blaser, J. Mol. Catal. A: Chem. **173**, 3 (2001).
- ³⁰F. Favier, E. C. Walter, M. P. Zach, T. Benter, and R. M. Penner, Science **293**, 2227 (2001).
- ³¹E. C. Walter, Surf. Interface Anal. **34**, 409 (2002).
- ³²J. Kong, M. Chapline, and H. Dai, Adv. Mater. (Weinheim, Ger.) **13**, 1384 (2001).
- ³³G. Schmid, M. Baumle, M. Geerkens, I. Helm, C. Osemann, and T. Sawitowski, Chem. Soc. Rev. **28**, 179 (1999).
- ³⁴Y. Volokitin, J. Sinzig, L. J. deJongh, G. Schmid, M. N. Vargaftik, and I. I. Moiseev, Nature (London) **384**, 621 (1996).
- ³⁵J. Westergren and S. Nordholm, Chem. Phys. **290**, 189 (2003).
- ³⁶S. M. Foiles, M. I. Baskes, and M. S. Daw, Phys. Rev. B **33**, 7983 (1986).
- ³⁷F. Ercolessi, E. Tosatti, and M. Parrinello, Philos. Mag. A **58**, 213 (1988); , Phys. Rev. Lett. **57**, 719 (1986).
- ³⁸D. Tomanek, A. A. Aligia, and C. A. Balseiro, Phys. Rev. B **32**, 5051 (1985).
- ³⁹A. P. Sutton and J. Chen, Philos. Mag. Lett. **61**, 139 (1990).
- ⁴⁰J. Uppenbrink and D. J. Wales, J. Chem. Phys. **98**, 5720 (1993).
- ⁴¹D. J. Wales and L. J. Munro, J. Phys. Chem. **100**, 2053 (1996).
- ⁴²L. D. Lloyd and R. L. Johnston, J. Chem. Soc. Dalton Trans. **3**, 307 (2000).
- ⁴³Z. A. Kaszkur and B. Mierzwa, Philos. Mag. A **77**, 781 (1998).
- ⁴⁴J. A. Nieminen, Phys. Rev. Lett. **74**, 3856 (1995).
- ⁴⁵E. J. Lamas and P. B. Balbuena, J. Phys. Chem. B **107**, 42 (2003).
- ⁴⁶W. Smith and T. R. Forester, DL_POLY; Daresbury Laboratory, Daresbury, UK, 1996.
- ⁴⁷M. P. Allen and D. J. Tildesley, *Computer Simulation of Liquids* (Clarendon Press, Oxford, 1987), p. 80.
- ⁴⁸L. Wang, Y. Zhang, X. Bian, and Y. Chen, Phys. Lett. A **310**, 197 (2003).
- ⁴⁹O. Glatter and O. Kratky, *Small Angle X-Ray Scattering* (Academic press, New York, 1982), p. 156.
- ⁵⁰M. K. Miller, *Atom Probe Tomography* (Kluwer Academic/Plenum Publisher, New York, 2000), p. 184.
- ⁵¹H. Reiss, P. Mirabel, and R. L. Whetten, J. Phys. Chem. **92**, 7241 (1988).
- ⁵²B. Rethfeld, K. Sokolowski-Tinten, D. von der Linde, and S. I. Anisimov, Phys. Rev. B **65**, 092103 (2002).
- ⁵³R. Kofman, P. Cheyssac, A. Aouaj, Y. Lereah, G. Deutscher, T. Bendavid, J. M. Penisson, and A. Bourret, Surf. Sci. **303**, 231 (1994).
- ⁵⁴Y. G. Chushak and L. S. Bartell, J. Phys. Chem. B **107**, 3747 (2003).
- ⁵⁵Y. Qi, T. Çağın, W. L. Johnson, and W. A. Goddard, J. Chem. Phys. **115**, 385 (2001).
- ⁵⁶F. Calvo and F. Spiegelmann, J. Chem. Phys. **112**, 2888 (2003).
- ⁵⁷O. Echt, K. Sattler, and E. Recknagel, Phys. Rev. Lett. **47**, 1121 (1981).
- ⁵⁸P. J. Steinhart, D. R. Nelson, and M. Ronchetti, Phys. Rev. B **28**, 784 (1983).
- ⁵⁹J. J. Sakurai and S. F. Tuan, *Modern Quantum Mechanics*, revised edition (Addison-Wesley, Reading, MA, 1994), p. 200.
- ⁶⁰Y. T. Wang and C. Dellago, J. Phys. Chem. B **107**, 9214 (2003).
- ⁶¹M. Jose-Yacamán, R. Herrera, A. Gomez, and S. Tehuacanero, Surf. Sci. **237**, 248 (1990).
- ⁶²S. C. Hendy and B. D. Hall, Phys. Rev. B **64**, 085425 (2001).
- ⁶³P. Buffat and J. P. Borel, Phys. Rev. A **13**, 2287 (1976).
- ⁶⁴T. Castro, R. Reifengerger, E. Choi, and R. P. Andres, Phys. Rev. B **42**, 8548 (1990).
- ⁶⁵J. G. Dash, Rev. Mod. Phys. **71**, 1737 (1999).
- ⁶⁶P. Pawlow, Z. Phys. Chem., Stoechiom. Verwandtschaftsl. **65**, 1 (1909); **65**, 545 (1909).
- ⁶⁷C. R. M. Wronski, Br. J. Appl. Phys. **18**, 1731 (1967).
- ⁶⁸H. Sakai, Surf. Sci. **351**, 285 (1996).
- ⁶⁹R. R. Vanfleet and J. M. Mochel, Surf. Sci. **341**, 40 (1995).
- ⁷⁰M. Wautelet, J. Phys. D **24**, 343 (1991).
- ⁷¹C. Q. Sun, Y. Wang, B. K. Tay, S. Li, H. Huang, and Y. B. Zhang, J. Phys. Chem. B **106**, 10701 (2002).
- ⁷²K. K. Nanda, S. N. Sahu, and S. N. Behera, Phys. Rev. A **66**, 013208 (2002).
- ⁷³*Chemistry and Physics of Solid Surface VII*, edited by R. Vanselow and R. Howe (Springer-Verlag, Berlin, 1988).
- ⁷⁴T. Iida and R. I. L. Guthrie, *The Physical Properties of Liquid Metals* (Clarendon Press, Oxford, 1988).